

ENERGY-INERTIAL SCALE INTERACTIONS FOR VELOCITY AND TEMPERATURE IN THE UNSTABLE ATMOSPHERIC SURFACE LAYER

GABRIEL KATUL, CHENG-I HSIEH and JOHN SIGMON
School of the Environment, Duke University, Durham, NC 27708-0328, U.S.A.

(Received in final form 16 July, 1996)

Abstract. Triaxial sonic anemometer velocity and temperature measurements were used to investigate the local structure of the velocity and temperature fluctuations in the unstable atmospheric surface layer above a grass-covered forest clearing. Despite the existence of a $2/3$ power law in the longitudinal velocity (2 decades) and temperature (1 decade) structure functions, local isotropy within the inertial subrange was not attained by the temperature field, although a near-isotropic state was attained by the velocity field. It was found that sources of anisotropy were due to interactions between the large-scale and small-scale eddy motion, and due to local velocity-thermal interactions. Statistical measures were developed and used to quantify these types of interactions. Other types of interactions were also measured but were less significant. The temperature gradient skewness was measured and found to be non-zero in agreement with other laboratory flow types for inertial subrange scales. Despite these interactions and anisotropy sources in the local temperature field, Obukhov's 1949 hypothesis for the mixed velocity-temperature structure functions was found to be valid. Finally, our measurements show that while a $2/3$ power-law in the longitudinal velocity structure function developed at scales comparable to five times the height from the ground surface (z), near-isotropic conditions were achieved at scales smaller than $z/2$.

1. Introduction

Numerous field and laboratory experiments demonstrate that velocity and temperature measurements in the atmospheric surface layer (ASL) exhibit an extensive inertial subrange, whose signature is commonly associated with a $-5/3$ power law in the spectral density function. Within the inertial subrange, turbulent kinetic energy per unit mass (TKE) is neither produced nor dissipated but simply cascades down to smaller scales by vortex stretching. An important statistical property of the inertial subrange is the locally isotropic nature of the eddy motion. This isotropy permits simplifications to the dynamical description of these scales of motion according to Kolmogorov's (1941) original theory (hereafter referred to as K41).

A wide inertial subrange in the ASL is attributed to the large-scale separation between turbulent production (mechanical and buoyant) at L_u and viscous dissipation at η . In this study, L_u is the integral length scale of the longitudinal velocity fluctuations, η ($=[\nu^3/\langle\epsilon\rangle]^{1/4}$) is the Kolmogorov microscale, ν ($= 1.5 \times 10^{-5} \text{ m}^2 \text{ s}^{-1}$) is the kinematic viscosity of air, ϵ ($=\nu[\partial u_i/\partial x_j + \partial u_j/\partial x_i]^2$) is the turbulent kinetic energy dissipation rate per unit mass, u_i is the turbulent velocity fluctuation component ($u_1 = u$, $u_2 = v$, and $u_3 = w$), $x_1(=x)$, $x_2(=y)$,

and $x_3(=z)$ are the longitudinal, lateral, and vertical directions, respectively (in this study, both meteorological and tensor notations are used), and $\langle \cdot \rangle$ is the time averaging operator (assumed to be identical to the ensemble averaging operator by the ergodic hypothesis as discussed in Monin and Yaglom, 1971; Ch. 2; Lumley and Panofsky, 1964). This wide separation between L_u and η (for many unstable ASL flows $L_u/\eta \approx 10^5$) ensures that the transfer of TKE ($= T_E$), from production to dissipation, cascades over many intermediate scales. Hence, it is expected that all anisotropy in the eddy motion associated with the turbulent production (mechanical or thermal) at L_u will diminish during this energy cascade process.

Air-temperature time series measurements in the ASL clearly exhibit well defined large-scale structures (e.g. temperature ramps) whose length scales are comparable or larger than L_u . The sharp edges of these structures, characterized by a large and rapid change in temperature over a very short time duration, may contribute directly to Fourier amplitudes at higher wavenumbers without many intermediate cascade steps, as evidenced by Mahrt (1989). Hence, when these structures exist, the inertial subrange eddy motion (hereafter referred to as small scale) may be contaminated by the larger scale organized eddy motion due to a “short circuiting” in the energy-cascade. While this non-local energy transfer is attributed to the rapid drop at the ramp-edge, other studies demonstrated that the ramp slopes are of significance. For example, Van Atta (1977) showed that the ramp-like structures in the temperature significantly contribute to the non-zero values of the odd-ordered temperature structure functions in agreement with Gibson *et al.* (1977). Based on local isotropy predictions, these odd-ordered temperature structure functions must be identically zero for all separation distances within the inertial subrange. To explain the non-zero behavior of the odd-ordered temperature structure functions, Van Atta (1977) proposed an idealized ramp model that implicitly assumes organized motion with ramp-like signatures influence the inertial subrange statistics of the temperature field.

Irrespective of the anisotropy source (ramp slope or edge), if interactions between large scales and small scales are significant, then it is possible that the anisotropy of the large scales persists in the inertial subrange, and key assumptions regarding i) isotropy, ii) the universal nature of the power-laws within the inertial subrange, (e.g. Kuznetsov *et al.*, 1992), and iii) Obukhov’s constant structure skewness hypothesis (Obukhov, 1949; Katul *et al.*, 1994a) are violated and require re-examination for ASL flows. If such interactions are important, then the structure of the inertial subrange may not be universal since the larger scale eddy motions are strongly influenced by the boundary conditions imposed by the land-atmosphere interface or the existing atmospheric stability conditions. For the purpose of this study, large scales are eddies with characteristic length scales $\geq L_u$ and small scales are eddies with scales much larger than η but much smaller than the height above the ground surface (z).

The objective of this study is to investigate the influence of such interactions on the Kolmogorov inertial scale eddy motion close to the land-atmosphere interface

using velocity and temperature time series measurements within the ASL. Special attention is paid to the local velocity-thermal interaction, an interaction that was investigated by Antonia and Van Atta (1975, 1978), Antonia and Chambers (1980), and recently by Antonia and Zhu (1994) who measured non-zero amplitudes in the longitudinal heat flux co-spectrum within the inertial subrange.

For that purpose, 56 Hz triaxial sonic anemometer velocity and temperature measurements were carried out in the ASL above a grass-covered forest clearing in Durham, North Carolina for a wide range of atmospheric stability conditions. Our specific objectives are to investigate how energy containing small-scale interactions and local velocity-thermal interactions modify i) K41 power-laws, ii) Obukhov's constant skewness hypothesis, and iii) the isotropic state of the small-scale eddy motion in the ASL. Since K41 and Obukhov's constant skewness hypothesis were developed for the velocity and temperature differences between two neighbouring points, the structure function approach is utilized throughout.

2. Theory

The equations relating the second ($D_{uu}(r)$) and third ($D_{uuu}(r)$) order structure functions, and the mixed velocity-temperature ($D_{TTu}(r)$) and second order temperature ($D_{TT}(r)$) structure functions, as derived from the Navier–Stokes (NS) equations for locally isotropic turbulence, are given by

$$\begin{aligned} D_{uuu}(r) - 6\nu \frac{d}{dr} D_{uu}(r) &= -\frac{4}{5} \langle \epsilon \rangle r \\ D_{TTu}(r) - 2\chi \frac{d}{dr} D_{TT}(r) &= -\frac{4}{3} \langle N_T \rangle r \end{aligned} \quad (1)$$

where $D_{uuu}(r) = \langle [u(x+r) - u(x)]^3 \rangle$, $D_{uu}(r) = \langle [u(x+r) - u(x)]^2 \rangle$, $D_{TT}(r) = \langle [T(x+r) - T(x)]^2 \rangle$, $D_{TTu}(r) = \langle [T(x+r) - T(x)]^2 [u(x+r) - u(x)] \rangle$, N_T is one half the temperature variance dissipation rate, χ is the molecular diffusivity for heat, and r is the separation distance along the longitudinal direction (see Monin and Yaglom, 1975, p. 401–403 for derivation). In deriving Equation (1), it is assumed that the Reynolds and Peclet numbers are very large, the statistical state of the small-scale eddies (e.g. scales much smaller than L_u) are independent of the macro-structural flow properties, and that the temperature and velocity differences (ΔT and Δu), for r much less than L_u and L_T , are independent. Here, L_T is the temperature integral length scale. That is, at the small scales, temperature is a passive scalar and does not interact locally with the longitudinal velocity field. Throughout this study, we will assume that at any time instant (t), the longitudinal velocity (U) and air temperature (T_a) can be decomposed, without ambiguity, into time averages ($\langle U \rangle$, $\langle T \rangle$) and fluctuations about these time averages (u , T). Thus, at time t , $U(t) = \langle U \rangle + u(t)$ and $T_a(t) = \langle T \rangle + T(t)$, and $\langle u_i \rangle = 0$.

An important asymptotic result that follows from Equation (1) is the behavior of $D_{uuu}(r)$ and $D_{TTu}(r)$ in the limit when $r \gg \eta$ and ν is very small. This is given by

$$\begin{aligned} D_{uuu}(r) &\simeq -\frac{4}{5}\langle\epsilon\rangle r \\ D_{TTu}(r) &\simeq -\frac{4}{3}\langle N_T \rangle r \end{aligned} \tag{2}$$

which agrees well with K41 ($=C_n(\langle\epsilon\rangle r)^{n/3}$) predictions for the third order ($n = 3$) longitudinal velocity structure function with $C_3 = -4/5$. Obukhov (1949) suggested that the following dimensionless quantities

$$\begin{aligned} S(r) &= \frac{D_{uuu}(r)}{[D_{uu}(r)]^{3/2}} \\ F(r) &= \frac{D_{TTu}(r)}{D_{TT}(r)[D_{uu}(r)]^{1/2}} \end{aligned} \tag{3}$$

to be constants independent of r in order to recover K41 predictions for $D_{uu}(r)$ and $D_{TT}(r)$ from $D_{uuu}(r)$ and $D_{TTu}(r)$ (see also Monin and Yaglom, 1975 pp. 397–400). These constants were determined experimentally to be $S(r) = -0.25$ and $F(r) = -0.4$ and were also related to the Kolmogorov constant as discussed in Katul *et al.* (1995a). Notable exceptions to these experimental values are due to Kerr (1985, 1990) who found $S(r) = -0.4$ and $F(r) = -0.5$ using a direct numerical simulation for isotropic turbulence (see also Gibson *et al.*, 1988). Also, the -0.4 value for $F(r)$ is not consistent with the accepted Kolmogorov constant for the second order temperature structure function $C_T = 3.2$ (see Kaimal and Finnigan, 1994; p. 52).

3. Experimental Setup

The measurements were carried out on July 12–16, 1995 at 5.2 m above the ground surface over an *Alta Fescue* grass site at the Blackwood division of the Duke Forest in Durham, North Carolina. During this time period, a heat wave resided in North Carolina for several days after it had swept from the midwest to the east coast. During the experiment, maximum mean air temperatures up to 38 °C were measured in Durham. The sky condition during these five days was clear with low to moderate winds.

The site is a 480 m by 305 m grass-covered forest clearing (site elevation = 163 m), and a mast, situated at 250 m and 160 m from the north-end and west-end portions of a 10 m Loblolly pine forest edge respectively, was used

to mount a triaxial sonic anemometer. The three velocity components (U_1 , U_2 , U_3) and air temperature were measured using a triaxial ultrasonic anemometer (Gill Instruments/1012R2). Sonic anemometers measure the velocity by sensing the effect of wind on the transit times of sound pulses travelling in opposite directions across a known instrument path distance d_{sl} ($= 0.149$ m in this study). A key disadvantage of sonic anemometers is the wavenumber (K) distortion due to averaging along the finite sonic path d_{sl} . This distortion is limited to separation distances $r \leq d_{sl}$ or $K \geq d_{sl}^{-1}$ (Wyngaard, 1981; this limit was erroneously quoted in Katul *et al.*, 1995a,b as $K \geq 2\pi d_{sl}^{-1}$ instead of $K \geq d_{sl}^{-1}$ for K in rad s^{-1}). The sampling frequency (f_s) and the sampling period (T_p) were 56 Hz and 19.5 minutes respectively, resulting in $N = 65,536$ measurements per velocity component. The 56 Hz sampling frequency is the maximum achievable frequency by the Gill sonic anemometer and is used in this experiment. The Gill anemometer was calibrated at the Department of Aeronautics and Astronautics wind-tunnel facility ($2.1 \text{ m} \times 1.5 \text{ m} \times 4.4 \text{ m}$) at Southampton University and tested for any transducer delays and flow distortions. Taylor's (1938) frozen turbulence hypothesis was used to convert time increments to space increments ($r = -\langle U \rangle t$). Since some averaging occurs for $r < d_{sl}$, the statistical analysis is limited to $r > d_{sl}$ but the full range of structure function measurements is shown.

From the 5-day experiment, more than 120 runs were collected. After inspection, only 6 runs were used in this study, which exhibited i) at least one decade of inertial subrange as identified by the $2/3$ power law in the longitudinal velocity structure function, ii) a temperature standard deviation (σ_T) in excess of 0.2 °C to insure adequate thermal agitation, iii) clear and identifiable time averages ($\langle U \rangle$ and $\langle T \rangle$) to permit decomposition into a mean and a fluctuating part without ambiguity, and iv) a turbulent intensity $I_u (= \sigma_u / \langle U_1 \rangle$, where σ_u is the root-mean squared longitudinal velocity) not exceeding 0.33 to minimize distortions resulting from Taylor's (1938) frozen turbulence hypothesis. Due to the low wind speeds during the 5-day period, I_u was greater than 0.3 for the majority of runs. For 30 runs, the wind speeds at 5.2 m were below 1.5 m s^{-1} . For near convective conditions, none of the runs had an $I_u < 0.33$ and we used the run with the smallest turbulent intensity ($I_u = 0.44$). Therefore, the total number of runs from this experiment is 7.

While the limiting $I_u = 0.33$ is well within the criteria set by Stull (1988 p. 6), this intensity is not very small (e.g. $I_u^2 = 0.1$) as evidenced by Lin (1953). We still employed Taylor's (1938) frozen turbulence hypothesis assuming that it is at least valid for the small-scale eddy motion within the inertial subrange. Powell and Elderkin (1974) and Mizuno and Panofsky (1975) did demonstrate that Lin's (1953) criterion ($I_u^2 \ll 0.1$) is too limiting for the ASL and can be relaxed for operational purposes. Despite an $I_u^2 = 0.09$, they found that Taylor's (1938) frozen turbulence hypothesis is valid for scales in excess of 250 m. We note that distortions at the small scales in high intensity shear flow can be severe, as shown by the experiments of Fisher and Davies (1964). A potential assessment of these

distortions is presented in the following section using the model by Wyngaard and Clifford (1977).

The absolute air temperature was determined from the speed of sound c_s using

$$c_s^2 = \alpha R_d T_a \quad (4)$$

where $R_d (=287.04 \text{ J Kg}^{-1} \text{ K}^{-1})$ is the gas constant of dry air at constant pressure, and $\alpha (= 1.4)$ is the ratio of the molar specific heat capacities of air at constant pressure to that at constant volume. It should be noted that the spatial averaging of the sonic anemometer for temperature readings are compatible with those for velocity. However, the temperature measurements are also contaminated by residual sensitivities to humidity. This was the main reason for considering runs with $\sigma_T > 0.2 \text{ }^\circ\text{C}$ to ensure that the temperature perturbations are large enough to be well detected by the sonic anemometer and we neglect the secondary humidity corrections to the temperature measurements (see also Kaimal, 1986). A comparison between the Gill temperature fluctuations and a Campbell Scientific fine wire chromel-constantan thermocouple is discussed in Appendix A. Good agreement between the temperature measurements from both instruments is noted in Appendix A. The characteristic turbulence length scales are summarized in Table I, where the longitudinal (L_u) and vertical (L_w) velocity, and temperature (L_T) integral length scales, the Taylor microscale (λ), and η were estimated from

$$\begin{aligned} L_T &= \frac{\langle U \rangle}{\langle T^2 \rangle} \int_0^\infty \langle T(t + \tau)T(t) \rangle d\tau \\ L_{u_i} &= \frac{\langle U \rangle}{\langle u_i^2 \rangle} \int_0^\infty \langle u_i(t + \tau)u_i(t) \rangle d\tau \quad i = 1, 3 \\ \lambda &= \sigma_u \sqrt{15 \frac{\nu}{\langle \epsilon \rangle}} \\ \eta &= \left(\frac{\nu^3}{\langle \epsilon \rangle} \right)^{1/4} \end{aligned} \quad (5)$$

(see Tennekes and Lumley, 1972 pp. 66–67). For determining L_u , L_w and L_T , the integration of the autocorrelation function was carried out up to the first zero crossing (see Sirivat and Warhaft, 1983). From Table I, the mean L_w and L_u are 2.0 m and 40.0 m, respectively, and are in excellent agreement with the estimates by Kader *et al.* (1989) who found $L_u/L_w = 20.6$. Due to the limited spatial resolution of sonic anemometers, the mean dissipation rate was not directly measured. However, $\langle \epsilon \rangle$ was estimated using two methods: i) similarity theory in conjunction with the steady state assumption that $T_E = \langle \epsilon \rangle$, and ii) the third order structure function. These methods are discussed next:

Table I

Summary of mean turbulence conditions: friction velocity (u_*), sensible heat flux (H), stability parameter (z/L), mean horizontal wind speed ($\langle U_1 \rangle$), wind direction (WD), velocity and temperature standard deviations ($\sigma_u, \sigma_v, \sigma_w, \sigma_T$), integral length scales (L_u, L_w, L_T), Taylor microscale (λ), and Kolmogorov dissipation length (η) are presented

Run No.	$\langle U_1 \rangle$ m s ⁻¹	I_u	z/L	u_* m s ⁻¹	H W m ⁻²	WD °N	σ_u m s ⁻¹	σ_v m s ⁻¹	σ_w m s ⁻¹	σ_T °C	L_u m	L_w m	L_T m	λ cm	η mm
1	2.59	0.33	-0.25	0.20	59.05	175	0.86	1.29	0.44	0.29	56.04	2.62	6.17	12.72	0.76
2	2.63	0.29	-0.32	0.18	60.01	107	0.75	0.96	0.42	0.31	31.25	2.17	5.76	12.93	0.82
3	2.90	0.30	-0.14	0.27	84.23	85	0.86	1.23	0.44	0.39	41.33	2.15	9.45	11.76	0.73
4*	2.07	0.44	-3.01	0.10	102.4	81	0.90	1.03	0.42	0.54	41.43	1.97	4.34	11.62	0.74
5	2.23	0.35	-0.16	0.25	72.72	51	0.78	0.79	0.35	0.35	37.29	1.44	5.53	12.26	0.78
6	2.47	0.33	-0.08	0.24	38.23	131	0.83	0.71	0.34	0.22	78.53	1.12	4.09	11.18	0.72
7	2.41	0.28	-0.37	0.17	57.22	135	0.69	0.76	0.34	0.34	31.77	1.92	5.74	14.15	0.89

* Turbulent intensity above 0.33. This run was included since it was the only near-convective run with a turbulent intensity below 0.45.

(i) Similarity Theory

The mean dissipation rate can be estimated from

$$\langle \epsilon \rangle = \left[\phi_\epsilon \left(\frac{z}{L} \right) \right] \frac{u_*^3}{kz} \quad (6)$$

where u_* ($= \langle -uw \rangle^{1/2}$) is the friction velocity, z ($= 5.2$ m) is the height above the ground surface, and L is the Obukhov length given by

$$L = - \frac{\rho u_*^3}{kg \left(\frac{H}{c_p T_a} \right)} \quad (7)$$

where H ($= \rho c_p \langle wT \rangle$) is the sensible heat flux, and ϕ_ϵ is the dissipation stability correction function (see Panofsky and Dutton, 1984 p. 180; Brutsaert, 1982 p. 193 for a review) given by the following empirical relations:

$$\begin{aligned} \phi_\epsilon &= 1 - \frac{z}{L}; & \left(\frac{z}{L} < 0 \right) \\ \phi_\epsilon &= \phi_m - \frac{z}{L}; \quad \phi_m = \left(1 - 16 \frac{z}{L} \right)^{-1/4}; & \left(-2 < \frac{z}{L} < 0 \right) \\ \phi_\epsilon &= \left(1 + 0.5 \left| \frac{z}{L} \right|^{2/3} \right)^{3/2}. & \left(-2 < \frac{z}{L} < 0 \right) \end{aligned} \quad (8)$$

Hence, from measured u_* and H , $\langle \epsilon \rangle$ can be determined for all dissipation stability correction functions; comparisons are shown in Table II.

(ii) The Third Order Structure Function

The mean dissipation rate was also determined from the measured third order structure function using the following procedure:

- (1) Utilize the dependence of $D_{uuu}(r)$ ($= -4/5 \langle \epsilon \rangle r$) on r to determine the extent of the inertial subrange, if it exists.
- (2) Fit a linear regression model of the form $D_{uuu}(r) = Ar$ and determine the slope (A) using linear regression analysis.
- (3) Compute $\langle \epsilon \rangle$ from the slope A (determined from linear regression analysis in step 2) using $\langle \epsilon \rangle = -5A/4$.

A similar procedure was used to estimate $\langle \epsilon \rangle$ from the measured $D_{uu}(r)$ and the Kolomogorov constant ($C_2 = 2.2$; see Kaimal and Finnigan, 1994 pp. 63–64). These estimates of $\langle \epsilon \rangle$ are compared to the estimates from method (i) in Table II. All methods result in comparable estimates of the mean dissipation rate, at least for the purpose of this study. We decided to use the estimated $\langle \epsilon \rangle$ from D_{uuu} for computing

Table II

Comparison between the estimated mean dissipation rates ($\text{m}^2 \text{s}^{-3}$) using similarity theory and the structure function approaches. The estimated dissipations using similarity theory are for the suggested stability correction functions. The subscripts 1, 2, and 3 are for the stability correction functions in Equation (8) starting from top to bottom, respectively. For the purpose of this study, the dissipation rates estimated from D_{uuu} are used to calculate λ and η in Table I

Run no.	Similarity theory			Structure function	
	$\langle \epsilon \rangle_1$	$\langle \epsilon \rangle_2$	$\langle \epsilon \rangle_3$	$\langle \epsilon \rangle$ from D_{uu}	$\langle \epsilon \rangle$ from D_{uuu}
1	0.0045	0.0033	0.0047	0.0096	0.0103
2	0.0038	0.0027	0.0039	0.0089	0.0076
3	0.0103	0.0080	0.0109	0.0087	0.0120
4*	0.0021	0.0018	0.0015	0.0083	0.0115
5	0.0082	0.0063	0.0087	0.0057	0.0091
6	0.0075	0.0062	0.0079	0.0064	0.0123
7	0.0032	0.0023	0.0033	0.0056	0.0053

* Turbulent intensity above 0.33. This run was included since it was the only near-convective run with a turbulent intensity below 0.45. Also, z/L is outside the range of stability conditions in (8).

λ since this dissipation method does not involve any assumption regarding planar homogeneity of the turbulence statistics (as in similarity theory) and is insensitive to the value of the Kolmogorov constant C_2 (as in D_{uu}). In this study, turbulence is considered to be planar homogeneous if the turbulence statistics do not vary in the longitudinal or lateral directions. The following analysis does not require explicit measures of $\langle \epsilon \rangle$ and we only report the dissipation rate here for calculating λ and η and qualitatively compare our results with other ASL and laboratory studies which report the Taylor microscale Reynolds number ($\text{Re} = \lambda \sigma_u / \nu$).

Using this estimate of $\langle \epsilon \rangle$, λ and η were computed from Equation (5). Also, for a qualitative order of magnitude evaluation, they were compared to ASL measurements by Bradley *et al.* (1981; Table I). For λ and η , Bradley *et al.* (1981) report a range from 0.056 m to 0.137 m and from 0.38 mm to 0.85 mm, respectively. It is interesting to note that the Bradley *et al.* (1981) measurements were carried out using a non-linearized DISA constant-temperature hot wire anemometer with a sampling frequency of 100 Hz. In their study, $\langle \epsilon \rangle$ was evaluated directly from the local isotropy relation in Tennekes and Lumley (1972 pp. 66; equation 3.2.9). These ranges are very similar to our indirect estimates in Table I. What is important to note from these estimates is that i) the termination of the inertial subrange, calculated by Praskovsky *et al.* (1993) to be 30η , is on the order of 3 cm and is well below the sonic anemometer path length, ii) separation distances close to d_{sl} may be comparable to λ , and iii) the Taylor microscale Reynolds number (see Table III) is well above 2,000, and the temperature field should achieve a near-isotropic state for small separation distances (see Jayesh *et al.*, 1994).

Table III

Summary of temperature and temperature gradient skewness. The longitudinal velocity skewness is also shown.

Run #	$\langle T^3 \rangle / (\sigma_T^3)$	$Re = \sigma_u \lambda / \nu$	$ S_T $
1	0.97	7,300	0.5
2	1.14	6,465	0.73
3	1.19	6,742	0.83
4*	1.08	7,572	0.88
5	0.43	6,375	0.80
6	0.45	5,187	0.71
7	0.63	6,507	0.58

* Turbulent intensity above 0.33. This run is in excellent agreement with the data by Gibson *et al.* (1977) for strongly unstable atmospheric conditions.

4. Results and Discussion

This section is divided into three parts, the first part discusses the extent of the inertial subrange and the onset of local isotropy, the second part presents the measured deviations from the Kolmogorov–Obukhov structure function equations and Obukhov’s (1949) hypothesis, the third part discusses these deviations within the context of large-scale/small-scale interactions and velocity-temperature interactions originally proposed in Praskovsky *et al.* (1993).

For the later purpose, the characteristic velocity of the small-scale eddy motion, defined within a sphere whose radius is $r (\ll L_u)$, is Δu (see also Frisch *et al.*, 1978; Monin and Yaglom, 1975 Ch. 8; Landau and Lifshitz, 1986 pp. 129–135; Katul *et al.*, 1995a,b). This scale is consistent with K41 since the dissipation rate, which defines all the velocity statistical properties within the inertial subrange, is on the order of $\Delta u^3 / r$ thus making Δu the appropriate small-scale velocity. Furthermore, it was shown in Praskovsky *et al.* (1993; Figures 8–10) that the large-scale characteristic velocity at a point is u . This velocity scale is consistent with the notion that at a point in the fluid, the amplitude of the turbulent perturbation is due to large-scale eddies. In this study, we assume that the same arguments hold for thermal perturbations.

4.1. IDENTIFICATION OF THE INERTIAL SUBRANGE AND THE ONSET OF LOCAL ISOTROPY

The identification of the inertial subrange is not a straightforward task given the wide range of tests and the different sensitivity levels of each test (see Antonia *et al.*, 1986 and Antonia and Kim, 1994). Saddoughi and Veeravalli (1994) presented

several methods to identify the low frequency limit at which an isotropic state in the velocity time series is achieved. They noted very different limits depending on the turbulent statistic being analyzed. In their study, the shear stress cospectral density function approached zero at wavenumbers about a decade larger than that at which the energy spectra first followed a $-5/3$ power law. Based on the Kansas experiments, Kaimal *et al.* (1972) found that the onset of local isotropy, as measured by the ratio of the vertical to the longitudinal velocity power spectrum, occurs at scales comparable to z . Their data show that for near-neutral conditions, the onset of local isotropy occurs at scales comparable to $0.5z$ (see also Kaimal, 1986). However, their data show a $-5/3$ power-law in the longitudinal velocity power spectrum at scales 5 times larger than z . The Praskovsky *et al.* (1993) data demonstrated that the inertial subrange, as identified by the third-order structure function, is between 30η and $L_u/8$. Kader *et al.* (1989) found that $L_u = 10.3z$ in the ASL, implying that the upper scale limit of Praskovsky *et al.* (1993) is about $1.3z$, which agrees with a $2\pi z/4.5$ theoretical estimate by Pond *et al.* (1963). A survey of isotropic limits from many other laboratory and ASL studies is presented in Monin and Yaglom (1975, pp. 453–458).

Since the structure function approach is used throughout this study, the relations between the vertical, lateral, and longitudinal velocity structure functions for locally isotropic turbulent flows are given by

$$\begin{aligned} \frac{D_{ww}(r)}{D_{vv}(r)} &= \frac{\langle (W(x+r) - W(x))^2 \rangle}{\langle (V(x+r) - V(x))^2 \rangle} = 1 \\ \frac{D_{uu}(r)}{D_{ww}(r)} &= \frac{\langle (U(x+r) - U(x))^2 \rangle}{\langle (W(x+r) - W(x))^2 \rangle} = \frac{3}{4} \end{aligned} \quad (9)$$

where $D_{ww}(r)$ and $D_{vv}(r)$ are the vertical and lateral velocity structure functions, respectively (see Monin and Yaglom, 1975 pp. 461). The above relations were used to investigate the inertial subrange isotropy rather than the ratio of the power spectra since for each separation distance (r), the structure function is calculated from at least 50,000 data points. In contrast, the average Fourier amplitudes for each wavenumber is calculated from a limited number of windows, and thus is noisier for the purpose of our study.

Also, the ratios in Equation (9) are less sensitive to possible distortion by Taylor's (1938) frozen turbulence hypothesis when compared to the $-5/3$ power-law in the individual longitudinal E_{uu} , lateral E_{vv} , and vertical E_{ww} velocity spectra. Notice in Equation (9) that any distortion caused by Taylor's (1938) hypothesis affects both the numerator and the denominator, and thus has less influence on their ratio, especially the lateral and vertical structure functions. In Figures 1a and 1b, the measured ratios in Equation (9) are presented for all seven runs. The lower scale limit is based on Wyngaard's (1981) sonic-anemometer distortion criteria ($r = d_{sl}$) and the upper limit is based on the Kaimal *et al.* (1972) data for near-

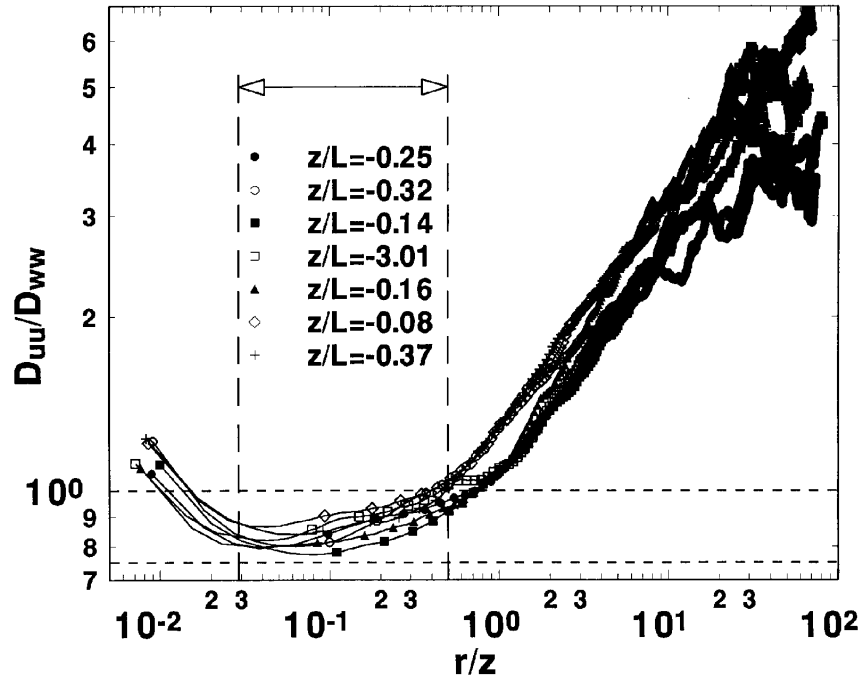


Figure 1a. The measured D_{uu}/D_{ww} as a function of the dimensionless separation distance (r/z) is shown for all 7 runs. The $3/4$ local isotropy predictions (horizontal, dotted) and the suggested inertial subrange limits (vertical dotted lines) from Kaimal *et al.* (1972) are also shown. For purposes of clarity, the data labelling frequency is 1 for every 20 measured points.

neutral conditions ($r = z/2$). For unstable atmospheric conditions, the Kaimal *et al.* (1972) data shows that $E_{ww}/E_{uu} = 4/3$ even at $r = z$.

Note in Figure 1a that D_{uu}/D_{ww} systematically overestimate the 0.75 predicted value from local isotropy assumptions. Interestingly, the Kansas E_{ww}/E_{uu} data in Kaimal *et al.* (1972) do show a marginal but systematic overshooting of the $4/3$ isotropy limit for unstable atmospheric stability conditions. In Figure 1b, the D_{ww}/D_{vv} data fluctuate around unity, but no clear systematic trend is evident. Whether this overestimation in Figure 1a is due to Taylor's (1938) hypothesis (especially its influence of D_{uu}) cannot be precisely assessed from one-point velocity measurements. However, some distortion estimation can be carried out using the model of Wyngaard and Clifford (1977). They extended an earlier analysis by Lumley (1965) to assess the distortions due to Taylor's (1938) hypothesis on the inertial subrange energy spectrum for a Gaussian isotropic velocity field in the absence of any interactions between large and small scales. They found that distortion corrections are on the order of $(1 + 11I_u^2/9)$ and $(1 + 11I_u^2/36)$ for E_{uu} and E_{ww} , respectively. Also, the corrections of Wyngaard and Clifford (1977) for the velocity spectra are wavenumber independent. Recall that the critical I_u is 0.33, and the maximum correction to E_{uu}/E_{ww} is 1.097, which is identical to the

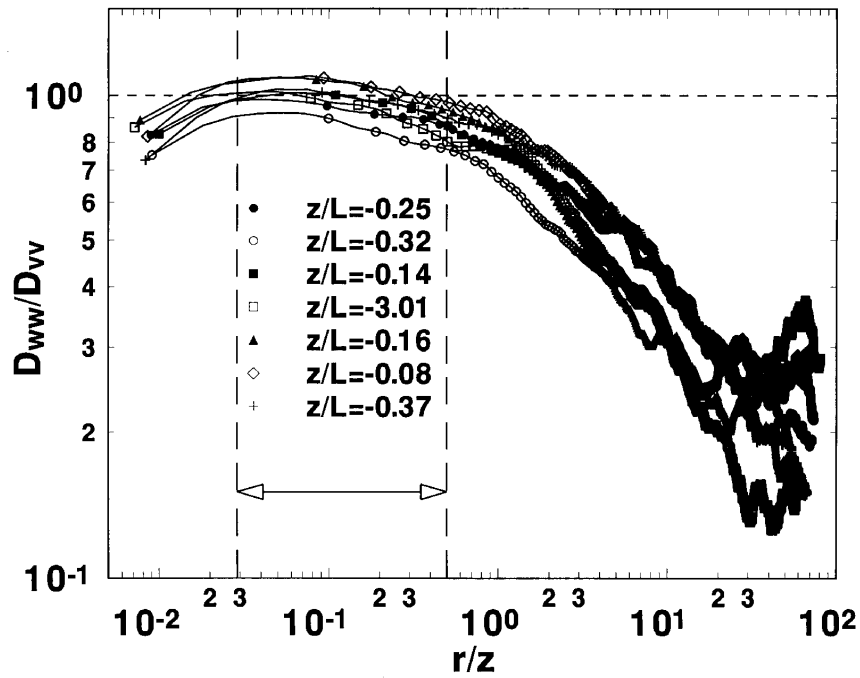


Figure 1b. Same as Figure 1a but for D_{ww}/D_{vv} .

correction ratio for D_{uu}/D_{ww} . Hence, by applying this correction to the 3/4 ratio (rather than adjusting the measured structure functions), the sonic anemometer measured isotropic limit should be 0.83 rather than 0.75, which agrees with the measurements in Figure 1a. Also, using the suggested relations by Wyngaard and Clifford (1977), the maximum distortions due to Taylor's (1938) hypothesis are about 13% for D_{uu} and 3% for D_{vv} and D_{ww} . As for distortion corrections to Figure 1b, we note that Wyngaard and Clifford's (1977) analysis assumes isotropic turbulence and the corrections to E_{vv} and E_{ww} (or D_{vv} and D_{ww}) are identical. Hence, no corrections to Figure 1b are necessary. Figure 1b appears to be best suited for identifying the inertial subrange since the ratio D_{ww}/D_{vv} is not very sensitive to distortions resulting from the application of Taylor's (1938) hypothesis. It also appears from Figure 1b that the limit suggested by the Kaimal *et al.* (1972) data for near-neutral conditions is in agreement with our measurements, and, for all practical purposes, defines the working limits for the inertial subrange and near isotropic state of the velocity field.

4.2. K41 POWER LAWS AND THE ONSET OF OBUKHOV'S CONSTANT SKEWNESS HYPOTHESIS

In this subsection, a comparison between the measured and predicted structure functions is presented as well as the measured deviations from Obukhov's hypoth-

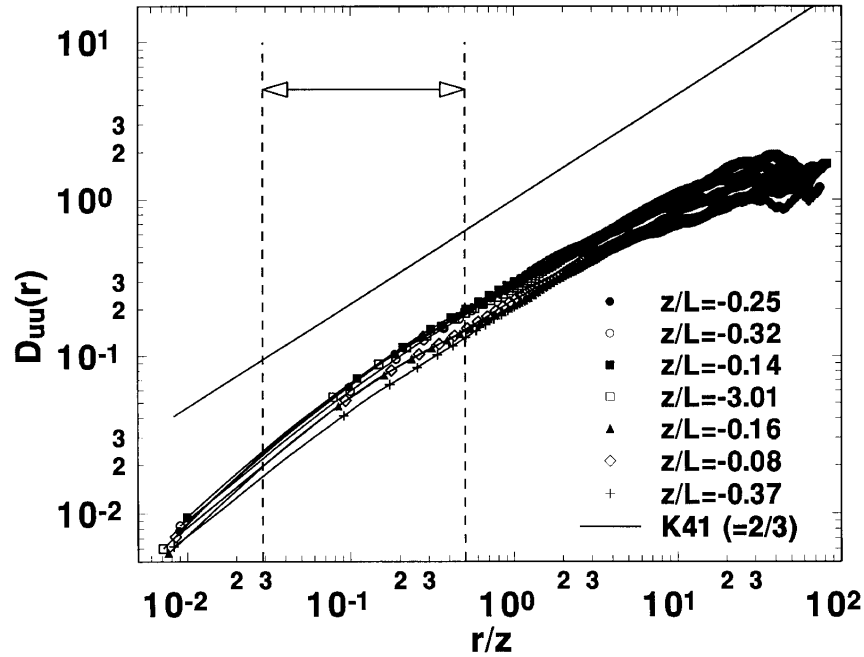


Figure 2a. The second-order structure function ($D_{uu}(r)$) as a function of the dimensionless separation distance (r/z). The $2/3$ power law is also shown (solid). For purposes of clarity, the data labelling frequency is 1 for every 20 measured points.

esis for velocity and temperature. Figures 2a and 2b display the measured second order structure functions for velocity and temperature respectively, for all seven runs. In both figures, it is apparent that for separation distances $r < d_{sl}$, the measured $D_{uu}(r)$ and $D_{TT}(r)$ slopes are steeper than K41 predictions due to the added dissipation by instrument volume averaging along d_{sl} . For $r > d_{sl}$, D_{uu} exhibited a $2/3$ power law consistent with K41 for at least $r > 5z$. This upper limit is in agreement with the limit found in Katul *et al.* (1995a,b) using $D_{uuu}(r)$. The D_{TT} in Figure 2b do not exhibit an extensive $2/3$ power law ($r = z$) when compared to $D_{uu}(r > 5z)$ in Figure 2a.

In order to assess Obukhov's (1949) hypothesis, the measured $S(r)$ and $F(r)$ are plotted against r/z for all runs in Figures 2c and 2d respectively. Notice that the scatter in Figure 2c is larger than the 0.22–0.3 variability reported from many laboratory experiments (see e.g. Townsend, 1976 pp. 98–99; Monin and Yaglom, 1975 pp. 471–473; Landau and Lifshitz, 1987 p. 145) but no consistent trend (i.e. overestimation or underestimation) is apparent. In this case, the scatter may be attributed to the limited sample size ($N = 65,536$) necessary to ensure convergence for $D_{uuu}(r)$. The average $S(r)$ from these seven runs is -0.2 , which is in close agreement with the $S(r) = -0.25$ (dotted line) derived from the Kolmogorov constant in Katul *et al.* (1995a; Appendix 3).

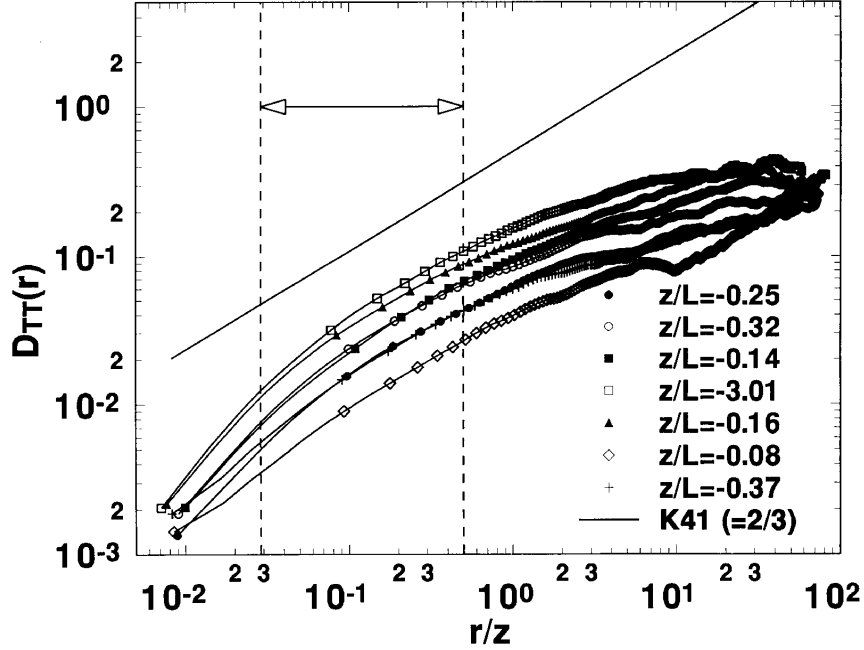


Figure 2b. Same as Figure 2a but for temperature ($D_{TT}(r)$).

Unlike $S(r)$, our $F(r)$ measurements are systematically lower than the suggested -0.4 value, indicating departure from Obukhov's (1949) hypothesis. However, we note that the $-F(r) = -0.4$ value is much higher than an $F(r)$ estimate strictly based on the Kolmogorov constants $C_2 = 2.2$ and $C_T = 3.2$ respectively, in conjunction with Equation (3) (e.g., $-F(r) = 0.28 = [4/3]/[3.2(2.2)^{0.5}]$). If $-F(r) = 0.28$ is adopted instead, all the measurements are still below the 0.28 expected value with the exception of the near-convective run. Nevertheless, the mean $-F(r)$ from all runs is 0.23 and it appears that Obukhov's (1949) hypothesis is a valid working approximation if $-F(r) = 0.28$ is used instead of the 0.4. Here we note that the internal intermittency corrections due to the averaging of the dissipation rate, in the sense of Kolmogorov (1962) or Frisch *et al.* (1978), are minor for the second-order structure function and are negligible for the third-order structure function. Hence, these refinements will not be treated in this study.

4.3. ENERGY-INERTIAL SCALE INTERACTIONS

It has been suggested by many investigators that the interaction between large scales and small scales are responsible for such deviations from K41 (see Kuznetsov *et al.*, 1992; Sreenivasan, 1991; Mahrt, 1989; Sreenivasan *et al.*, 1979; Van Atta, 1977). In the following section, we focus on five potential types of interactions: i) the influence of the large-scale eddy motion on the small-scale eddy motion, ii) the

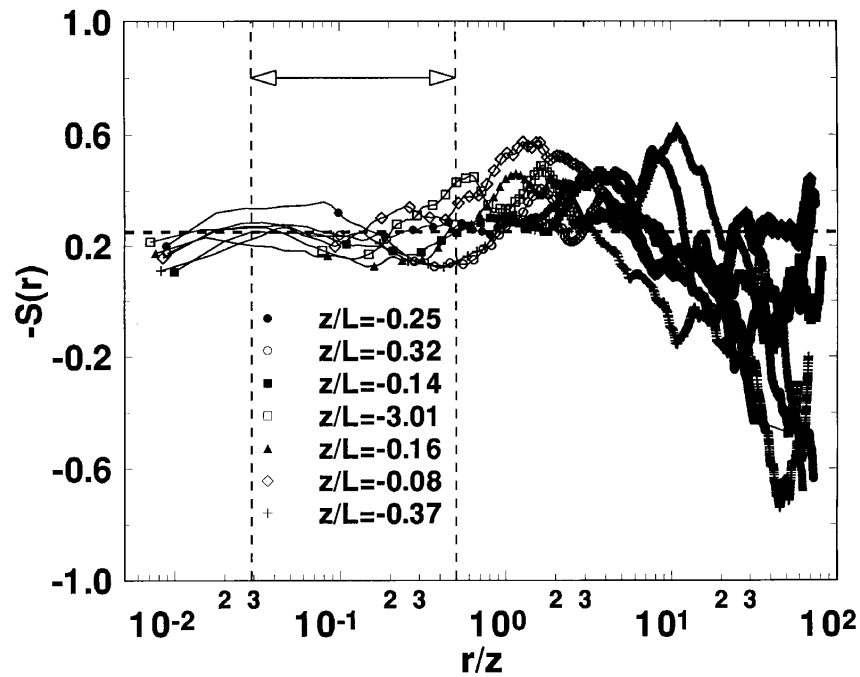


Figure 2c. The structure skewness $S(r)$ as a function of the dimensionless separation distance (r/z). $S(r)$ is constant for a locally isotropic turbulent flow. The -0.25 suggested value for locally isotropic turbulent flows is also shown (dotted line). For purposes of clarity, the data-labelling frequency is 1 for every 20 measured points.

influence of the large-scale thermal agitation on the small-scale thermal motion, iii) the influence of the small-scale thermal agitation on the small scale eddy motion, iv) the influence of the large-scale thermal agitation on the small-scale eddy motion, and v) the influence of large-scale velocity on local thermal interactions. Statistical measures were developed to quantify such interactions. Recall that K41 and the Kolmogorov–Obukhov structure function equations assume that all of the above interactions are negligible.

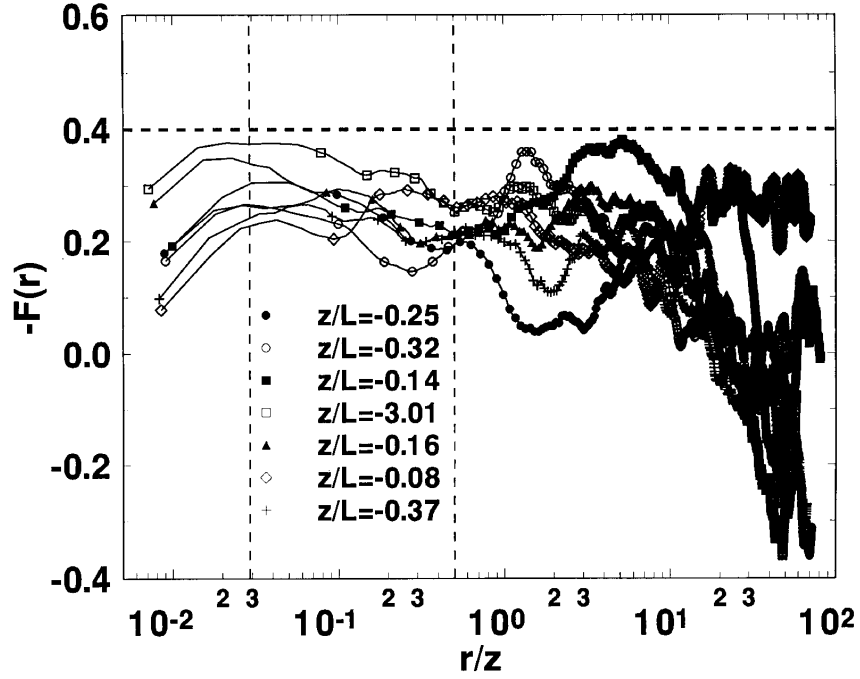


Figure 2d. The normalized mixed temperature-velocity structure function $F(r)$ as a function of the dimensionless separation distance (r/z). The suggested -0.4 value for locally isotropic turbulent flows is also shown (dotted line). For purposes of clarity, the data-labelling frequency is 1 for every 20 measured points.

4.3.1. Large Scale and Small Scale Longitudinal Velocity Interaction

A suggested measure of the net interaction between the large scale eddy motion (u) and the small scale eddy motion (characterized by Δu) is given by the correlation coefficient $\rho_{u,\Delta u}$

$$\rho_{u,\Delta u}(r) = \frac{\langle (u(x) - \langle u(x) \rangle)(\Delta u(x, r) - \langle \Delta u(x, r) \rangle) \rangle}{\sigma_u \sigma_{\Delta u}} \quad (10)$$

where σ_x is the standard deviation of the flow variable x and is given by

$$\sigma_x = \langle (x - \langle x \rangle)^2 \rangle^{1/2}. \quad (11)$$

Since $\langle \Delta u \rangle = \langle u \rangle = 0$ and $\Delta u = u(x+r) - u(x)$, Equation (10) simplifies to:

$$\rho_{u,\Delta u} = \frac{\langle u(x)u(x+r) \rangle - \langle u(x)^2 \rangle}{\langle u^2 \rangle^{1/2} (\langle u(x+r)^2 \rangle + \langle u(x)^2 \rangle - 2\langle u(x+r)u(x) \rangle)^{1/2}}. \quad (12)$$

Notice that Equation (12) implies two asymptotic limits for $\rho_{u,\Delta u}$.

1) For large separation distances (e.g. $r \gg L_u$), $\langle u(x+r)u(x) \rangle = 0$, and Equation (12) reduces to

$$\rho_{u,\Delta u} = \frac{-1}{\sqrt{2}} \simeq -0.707 \quad (13)$$

for planar homogeneous turbulence since $\langle u(x)^2 \rangle = \langle u(x+r)^2 \rangle$.

2) For very small separation distances (i.e. $r/z \rightarrow 0$), $\langle u(x)^2 \rangle \approx \langle u(x+r)^2 \rangle \approx \langle u(x+r)u(x) \rangle$. Hence, both numerator and denominator in Equation (12) approach zero. The limit of $x/(x^{1/2}) \rightarrow 0$ as $x \rightarrow 0$, and thus, $\rho_{u,\Delta u} \rightarrow 0$.

Within the inertial subrange, Equation (12) can be related to the velocity autocorrelation function $\rho(r) = \langle u(x+r)u(x) \rangle / \sigma_u^2$ using

$$\rho_{u,\Delta u} = -\frac{1}{\sqrt{2}} \sqrt{1 - \rho(r)}. \quad (14)$$

However, as shown in Monin and Yaglom (1975, pp. 85), the autocorrelation function and the structure function are related by

$$D_{uu}(r) = 2\sigma_u^2(1 - \rho(r)). \quad (15)$$

Replacing Equation (15) in Equation (14), using K41 to describe D_{uu} , and simplifying, gives

$$\rho_{u,\Delta u} = -\frac{1}{\sqrt{2}} \left(\frac{C_2}{2\sigma_u^2} \langle \epsilon \rangle^{2/3} r^{2/3} \right)^{1/2} \quad (16)$$

where $C_2 = 2.2$ is the Kolmogorov constant. To estimate the maximum magnitude of this correlation for inertial subrange scales with K41 theory, we first consider the neutral ASL with $\langle \epsilon \rangle = u_*^3/kz$, and $\sigma_u/u_* = 2.7$ (see Kader and Yaglom, 1990). With these estimates, Equation (16) simplifies to

$$\rho_{u,\Delta u} \approx -\frac{1}{\sqrt{2}k^{1/3}} \frac{u_*}{\sigma_u} \left(\frac{r}{z} \right)^{1/3}. \quad (17)$$

In K41, r is typically defined for scales much smaller than z so that implicit in K41 is the assumption that r/z is very small, and hence, $\rho_{u,\Delta u} \rightarrow 0$. In our ASL experiments, r/z varies between 0.03 to 0.5 so that we expect a non-zero $\rho_{u,\Delta u}$ that varies between -0.11 and -0.28 . We carried out similar analysis for unstable runs and found that the neutral runs yielded the largest absolute correlation coefficient ($= 0.28$) for $\rho_{u,\Delta u}$. Recall that σ_u/u_* is larger than 2.7 for the unstable ASL. Hence, if $|\rho_{u,\Delta u}|$ exceeds 0.28, then the large-scale eddy motion is contaminating the inertial subrange. Figure 3a displays the measured $\rho_{u,\Delta u}$ as a function of r/z for all runs. From Figure 3a, we note the following:

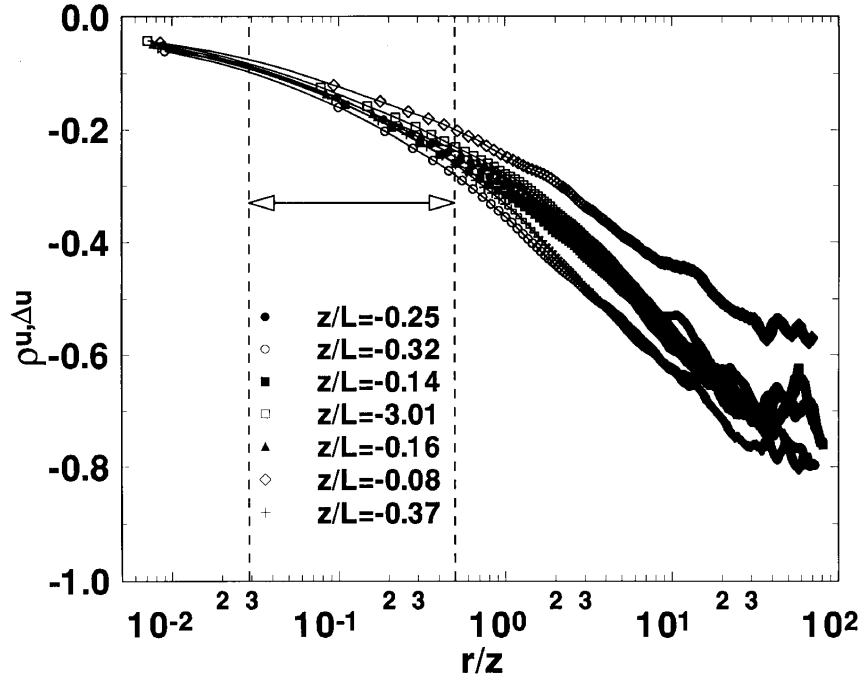


Figure 3a. The variation of $\rho_{u,\Delta u}$ as a function of r/z for all runs. The dotted vertical lines define the inertial subrange limits. For locally isotropic turbulence, the maximum $|\rho_{u,\Delta u}| = 0.28$.

- (1) $|\rho_{u,\Delta u}|$ is maximum for $r \geq L_u$ ($L_u \approx 10z$, see Table I). This is in agreement with the fact that the maximum interaction should occur at scales comparable to the turbulent production length scale ($= L_u$). Notice that for these large separation distances, $\rho_{u,\Delta u}$ is close to the -0.707 as predicted from Equation (13).
- (2) While $\rho_{u,\Delta u}$ is not zero for $r/z < 0.5$, it is smaller than 0.28 and consistent with the isotropy limits in Figure 1a and the calculations in Equation (17).

The fact that $\rho_{u,\Delta u}$ is non-zero within the inertial subrange suggests that the statistical properties of Δu might be weakly influenced by the statistical properties of u . This weak interaction, which will always exist within the inertial subrange for separation distances larger than λ , might explain the external intermittency effects on K41 reported in Kuznetsov *et al.* (1992). As stated in Kolmogorov (1941; definition 1), the probability density function $P_r(\Delta u)$ must be independent of the time-space origin and the velocity statistics at a point. Hence, a direct consequence of K41 is the equality $P_r(\Delta u | u) = P_r(\Delta u)$. This equality may not strictly hold if $|\rho_{u,\Delta u}|$ is large. Also, this analysis supports the conclusions made by Sreenivasan (1991) that weak anisotropy at the small scales might exist despite a wide scale separation between L_u ($> 10z$ in this study) and η . Using an X-wire anemometer at the Air Force Cambridge Research Laboratories, Busch (1973) found that local

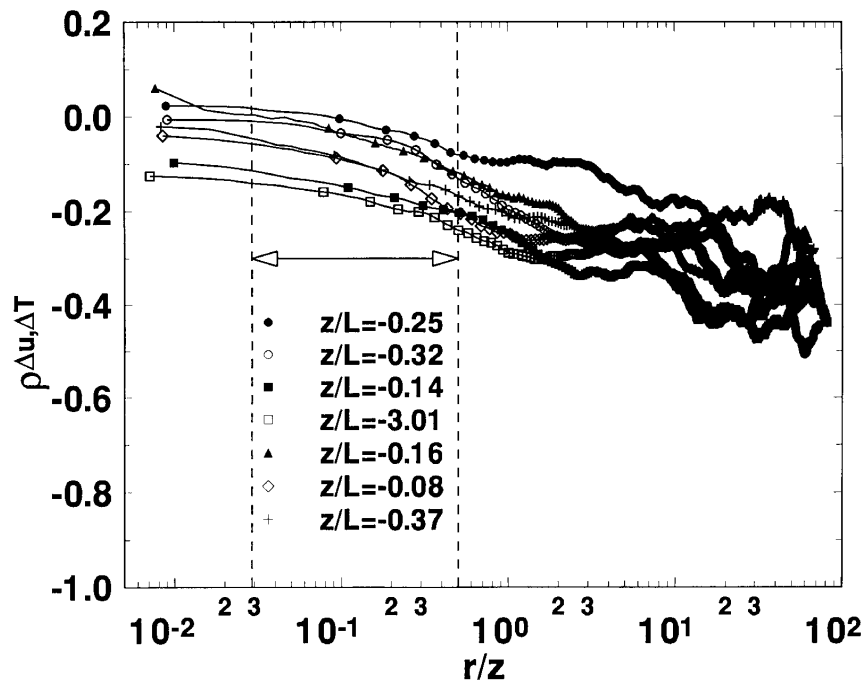


Figure 3b. Same as Figure 3a but for $\rho_{\Delta u, \Delta T}$. For locally isotropic turbulence, $\rho_{\Delta u, \Delta T} = 0$.

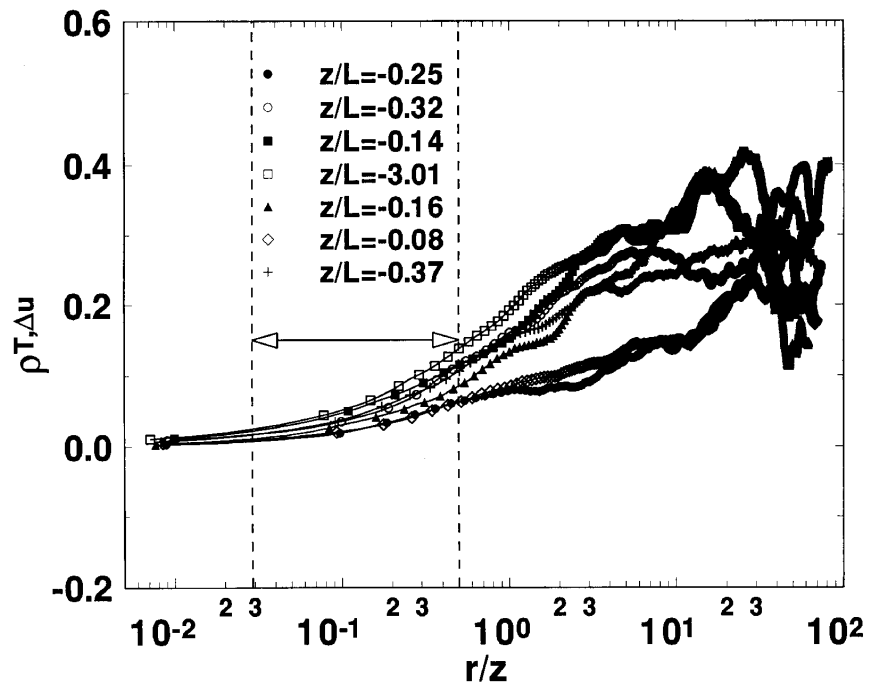


Figure 3c. Same as Figure 3a but for $\rho_{T, \Delta u}$. For a locally isotropic turbulence, $\rho_{T, \Delta u} = 0$.

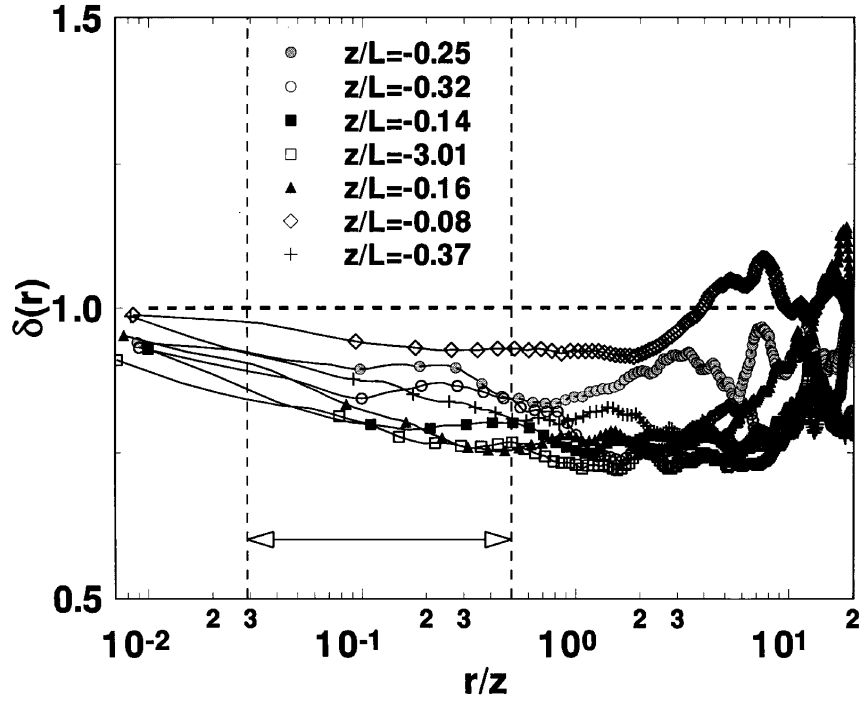


Figure 3d. Same as Figure 3a but for $\delta(r)$. For locally isotropic turbulence, $\delta(r) = 1$ (thick dotted line).

isotropy at 5.66 m above the ground surface is attained at wavenumbers much higher than that reported by Kaimal *et al.* (1972) despite the presence of a $-5/3$ power law in both data sets. A detailed laboratory boundary-layer study by Mestayer (1982) supports the absence of local isotropy within the inertial subrange in agreement with Busch (1973). Also, these results are in agreement with earlier measurements above a uniform bare soil surface by Katul *et al.* (1994a,b). However, what is important to note is that while these isotropy departures have been documented in several studies, these departures are not very large, as evidenced by Figures 1a, 1b, 2a and 3a. For a first-order analysis, the velocity statistics can be predicted from isotropic relations in the inertial subrange.

4.3.2. Longitudinal Velocity-Thermal Interaction at the Small Scales

A measure of the net interaction between the small scale temperature field and the small scale longitudinal velocity field is given by the correlation coefficient $\rho_{\Delta T, \Delta u}$

$$\rho_{\Delta T, \Delta u}(r) = \frac{\langle (\Delta T(x, r) - \langle \Delta T(x, r) \rangle) (\Delta u(x, r) - \langle \Delta u(x, r) \rangle) \rangle}{\sigma_{\Delta T} \sigma_{\Delta u}}. \quad (18)$$

The absence of any net interaction requires $\rho_{\Delta T, \Delta u}$ to be zero. As shown by Monin and Yaglom (1975, pp. 99–105), in a locally isotropic turbulence field

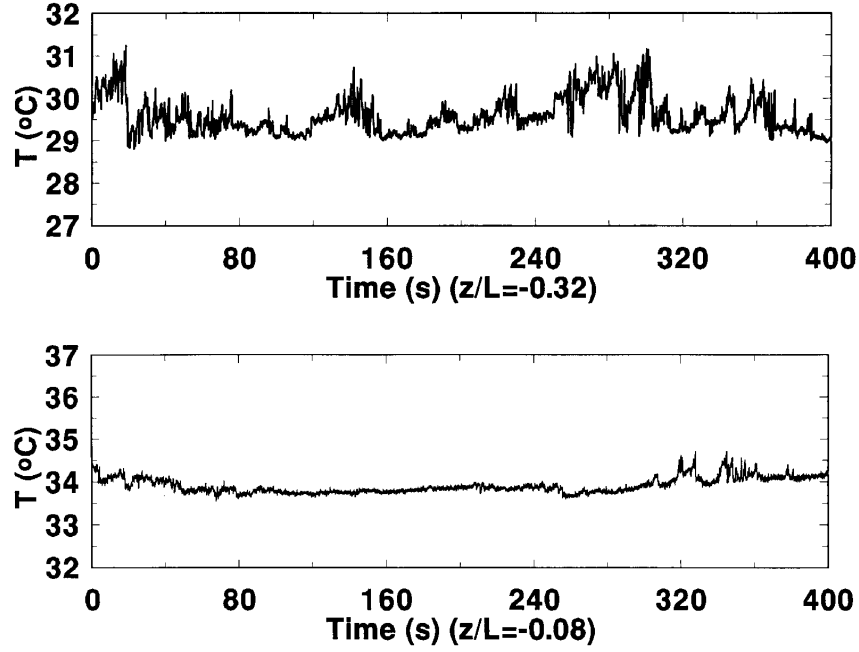


Figure 3e. The signature of ramp like patterns in the temperature time series for unstable ($z/L = -0.32$; upper figure) and near-neutral ($z/L = -0.08$; lower figure) atmospheric stability conditions.

$\rho_{\Delta T, \Delta u}$ must vanish in order to derive (1). We use this correlation to measure local thermal effects on the longitudinal velocity inertial subrange eddy motion. Figure 3b displays $\rho_{\Delta T, \Delta u}$ as a function of r/z for up to 100. Notice that $\rho_{\Delta T, \Delta u}$ is not zero within the inertial subrange and a key assumption in the derivation of the Kolmogorov-Obukhov structure function equation is violated. Also, the fact that $\rho_{\Delta T, \Delta u}$ is finite further supports the conclusions by Antonia and Zhu (1994) regarding the role of temperature-velocity interactions and the anisotropy in the temperature field. These conclusions were derived from the non-zero measured values of the longitudinal heat flux co-spectrum.

4.3.3. Influence of Large Scale Thermals on the Small Scale Eddy Motion

A measure of the net interaction between the large scale temperature field and the small scale longitudinal velocity is given by the correlation coefficient $\rho_{T, \Delta u}$

$$\rho_{T, \Delta u}(r) = \frac{\langle (T(x) - \langle T(x) \rangle)(\Delta u(x, r) - \langle \Delta u(x, r) \rangle) \rangle}{\sigma_T \sigma_{\Delta u}}. \quad (19)$$

The absence of any net interaction between the large scale temperature and small scale velocity fluctuations requires $\rho_{T, \Delta u}$ to be zero. If this correlation is finite, then the anisotropy characterizing the large scale thermal motion directly contributes to the small scale eddy motion of the longitudinal velocity. Hence, any interaction

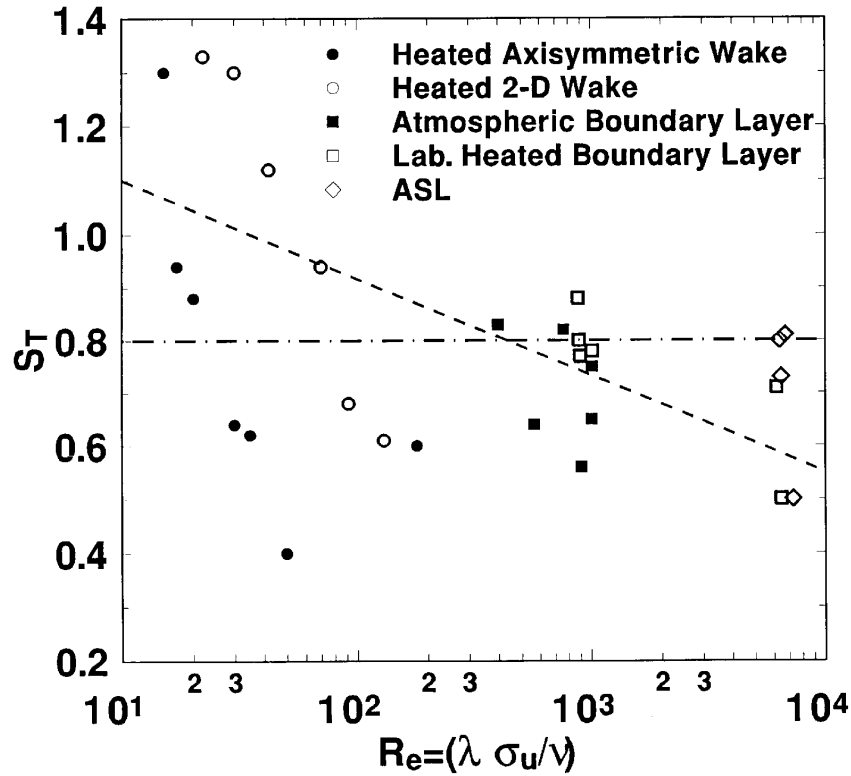


Figure 3f. The temperature skewness derivative as a function of the Taylor microscale Reynolds number. $S_T = 0.8$ is from Sreenivasan *et al.* (1979) and the dotted line is from Sreenivasan (1991).

between T and Δu indicates that local isotropy is not achieved. Figure 3c displays $\rho_{T,\Delta u}$ as a function of r/z for dimensionless separation distances up to 100. Notice from Figure 3c that $\rho_{T,\Delta u}$ is nearly zero within the inertial subrange and that large-scale thermal disturbances do not influence the local structure of the velocity field. This is qualitatively consistent with Figure 1a which shows that departures from $3/4$ do not depend on atmospheric stability conditions.

4.3.4. Influence of Large Scale Thermals on the Small Scale Thermal Motion

It was pointed out by Sreenivasan *et al.* (1979) that ramp-like structures directly contribute to the inertial subrange of the temperature field without intermediate cascading steps, and therefore, may directly contribute to inertial subrange anisotropy in the T_a measurements. Such conclusions are in agreement with the ramp-like phenomenological model discussed by Van Atta (1977). If the ramp-like patterns are important to the anisotropy of the small-scale motion, then it is possible to evaluate this interaction from the correlation between T and ΔT using the same derivation as in u and Δu . However, unlike the velocity field, it is difficult to establish an upper limit for this interaction based on K41 since both the TKE and

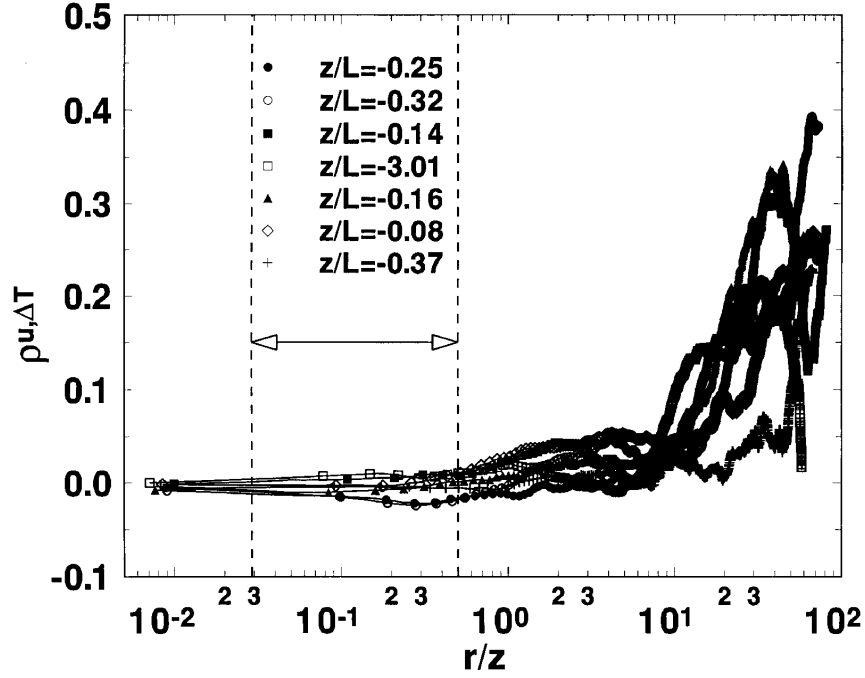


Figure 3g. Same as Figure 3a but for $\rho_{u,\Delta T}$. For locally isotropic turbulence, $\rho_{u,\Delta T} = 0$.

the thermal dissipation rates are needed. For this purpose, a separate analysis for the temperature field was developed and is summarized below:

(1) Expand the covariance $\langle T\Delta T^2 \rangle$ using

$$\langle T(x)[T(x+r) - T(x)]^2 \rangle = \langle T(x)T(x+r)^2 \rangle - 2\langle T(x+r)T(x)^2 \rangle + \langle T(x)^3 \rangle \quad (20)$$

and carry out the following simplifications by noting that:

(i) the mean temperature gradient skewness, defined as

$$S_T(r) = \frac{|\langle (T(x+r) - T(x))^3 \rangle|}{(D_{TT}(r))^{3/2}}, \quad (21)$$

is zero for locally homogeneous and isotropic turbulence (Sreenivasan, 1991), so that

$$\begin{aligned} \langle [T(x+r) - T(x)]^3 \rangle &= \langle T(x+r)^3 \rangle - 3\langle T(x+r)^2 T(x) \rangle \\ &\quad + 3\langle T(x+r) T(x)^2 \rangle + \langle T(x)^3 \rangle = 0, \end{aligned} \quad (22)$$

(ii) the third moment $\langle T(x)^3 \rangle$ is identical to $\langle T(x+r)^3 \rangle$ for locally homogeneous turbulence so that Equation (21) reduces to

$$\langle T(x+r)^2 T(x) \rangle = \langle T(x)^2 T(x+r) \rangle, \quad (23)$$

(2) use the identity in Equation (23) to simplify Equation (20). After several algebraic steps, Equation (20) reduces to

$$\langle T \Delta T^2 \rangle = - \langle T^2 \Delta T \rangle, \quad (24)$$

and, hence, a dimensionless measure $\delta(r)$ defined as

$$\delta(r) = - \frac{\langle T^2 \Delta T \rangle}{\langle T \Delta T^2 \rangle}, \quad (25)$$

must be unity for locally isotropic turbulence. Notice that Equation (25) is defined by the ratio of two covariances: the covariance ($\langle T \Delta T^2 \rangle$) measures the mean influence of large-scale temperature perturbations (T) on the local thermal energy (ΔT^2) while the second covariance ($\langle T^2 \Delta T \rangle$) measures the mean influence of local thermal perturbations (ΔT) on large-scale thermal energy (T^2). As evidenced from Equation (24), local isotropy requires a balance between these two covariances. Figure 3d shows the variation of $\delta(r)$ for all runs. Notice in Figure 3d that $\delta(r)$ is systematically less than unity suggesting that the interaction described by $\langle T \Delta T^2 \rangle$ is larger than the interaction described by $\langle T^2 \Delta T \rangle$. Whether the departure of $\delta(r)$ from unity is due to the ramp-like motion can be qualitatively assessed from Figures 3e and 3d. The signatures of ramp-like patterns in the temperature time series for unstable ($z/L = -0.32$; upper figure) and near-neutral ($z/L = -0.08$; lower figure) conditions are shown in Figure 3e. It is evident that an apparent ramp-like signature (upper figure) results in a stronger $\delta(r)$ departure from unity (see Figure 3d) when compared to the weak ramp-like signature (lower figure).

To further compare our measurements with other laboratory studies, especially studies that considered the influence of ramp-like motion on the temperature gradient skewness in the inertial subrange, we computed $|S_T|$ and compared our measurements with data from Gibson *et al.* (1977), Sreenivasan *et al.* (1979), and Sreenivasan (1991) in Figure 3f. Recall that a zero $|S_T|$ is central to $\delta(r) = 1$. Notice that the data in Figure 3f are not exclusively boundary-layer flows. The Taylor microscale Reynolds number ($\text{Re} = \sigma_u \lambda / \nu$) for many ASL flows are 3–10 times larger than many laboratory boundary-layer flows. Recall that for a locally isotropic temperature field, $S_T = 0$. The ASL values in Figure 3f were obtained by averaging the measured S_T values between $0.1 < r/z < 0.2$ and are summarized in Table III. This range was chosen for all seven runs since i) D_{TT} exhibits a $2/3$ power-law, ii) $r > 3d_{sl}$ and is well within the sonic anemometer temperature resolution, and iii) $r < 0.1 L_T$ so that one decade of cascade steps have occurred. Within this range, about 10 to 15 S_T values were averaged. The $S_T = 0.8$ constant temperature skewness is from Gibson *et al.* (1977) and Sreenivasan *et al.* (1979), and the dashed line is an extrapolation from the data by Sreenivasan (1991). Notice in Figure 3f that S_T is not zero for all runs (Run 4 was excluded from this comparison due to the large I_u) and that our ASL measurements are very comparable to the heated boundary-layer laboratory data in Sreenivasan (1991).

4.3.5. Influence of Large Scale Velocity on the Small Scale Thermal Motion

Based on the methodology previously proposed, this interaction can be characterized by the correlation coefficient between u and ΔT so that,

$$\rho_{\Delta T, u}(r) = \frac{\langle (u(x) - \langle u(x) \rangle)(\Delta T(x, r) - \langle \Delta T(x, r) \rangle) \rangle}{\sigma_u \sigma_{\Delta T}}. \quad (26)$$

Again, K41 and the Kolmogorov–Obukhov structure function for temperature assume that this correlation is zero. In Figure 3g, $\rho_{\Delta T, u}$ is displayed for all runs. From Figure 3g, note that $\rho_{\Delta T, u}$ is nearly zero for separation distances up to $10z$. Hence, Figure 3g suggests that the large scale velocity field and the small scale thermal disturbances are, to a first approximation, uncoupled within the inertial subrange.

5. Conclusions

This study has examined the local structure of velocity and temperature close to the ground surface. Despite the wide separation between production and dissipation length scales, an inertial subrange, in the sense of Kolmogorov’s local isotropy, was not observed for the temperature field despite two decades of $2/3$ power law in the longitudinal velocity structure function. Departures from K41 scaling and local isotropy predictions were investigated for velocity and temperature by assuming that the source of anisotropy is due to large scale–small scale interactions: For quantifying such interactions, the following were considered:

- [1] large scale–small scale velocity interactions.
- [2] local velocity–temperature interactions.
- [3] large scale temperature–local velocity interactions.
- [4] large scale temperature–local temperature interactions.
- [5] large scale velocity–local temperature interactions.

Special statistical measures were developed to quantify these interactions as a function of scale (or separation distances). Here, we label and refer to the above types of interactions as [1] to [5] respectively. Applying these statistical measures to the temperature and velocity time series, the following conclusions were derived:

- i) While the interactions described in [1], [3], [4], and [5] decrease with decreasing scale, the interaction in [2] appears to persist even at the smallest scales resolved by the triaxial sonic anemometer. The zero interaction in [2] is a necessary condition for Obukhov’s (1949) hypothesis for the mixed velocity temperature structure function.
- ii) The temperature gradient skewness was measured and was found to be non-zero in agreement with many laboratory studies that included heated axisymmetric wakes, heated two-dimensional wakes, and heated boundary layers.

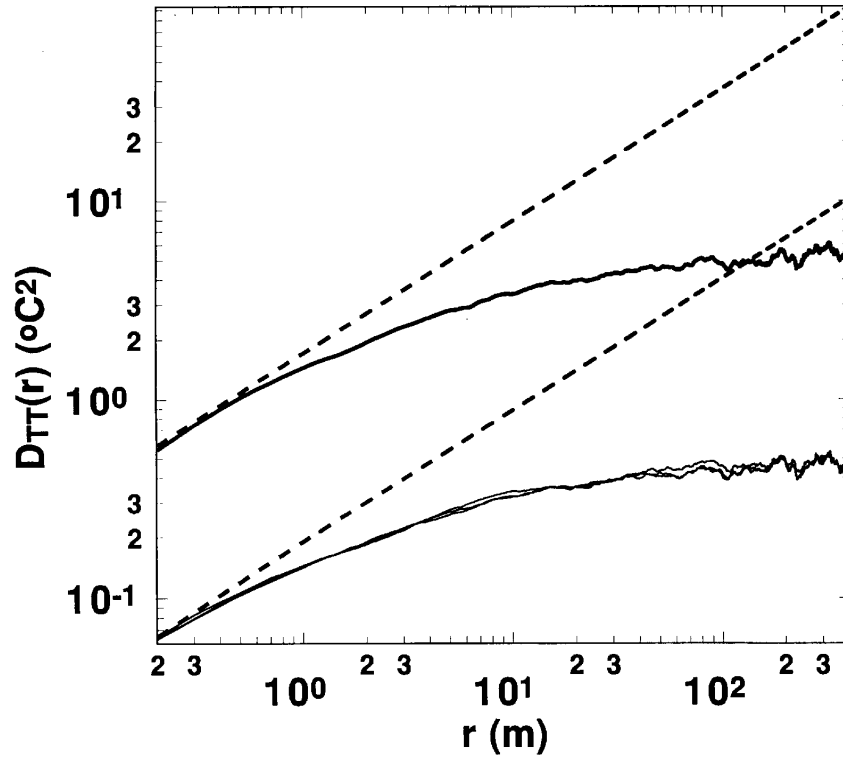


Figure 4a. Comparison between triaxial sonic anemometer and thermocouple second order temperature structure function (D_{TT}) for $\langle U \rangle = 2.16 \text{ m s}^{-1}$. The $2/3$ power law is also shown. The sonic anemometer structure function is shifted upward one decade to permit comparison at small separation distances.

The consequence of the non-zero temperature gradient skewness was further formulated in terms of an imbalance between two covariances that measure the interaction between the local thermal energy and the large-scale temperature perturbation, and the large-scale thermal energy and the local thermal perturbation. It was shown that for a locally isotropic temperature field, these two covariances must be identical. Our measurements showed that the interaction between the local thermal energy and the large-scale temperature perturbation is systematically larger than the large-scale thermal energy–local thermal perturbation interaction.

- iii) The fact that the local velocity and thermal eddy motion interact at the small scales also suggests that local isotropy in the temperature field may not be fully attained close to the ground surface despite the presence of a $2/3$ power law in the longitudinal velocity structure function. This finite interaction is in agreement with recent measurements by Antonia and Zhu (1994). However, it was also shown that such interactions result in minor departures from Obukhov's (1949) hypothesis for the mixed velocity-temperature structure function.

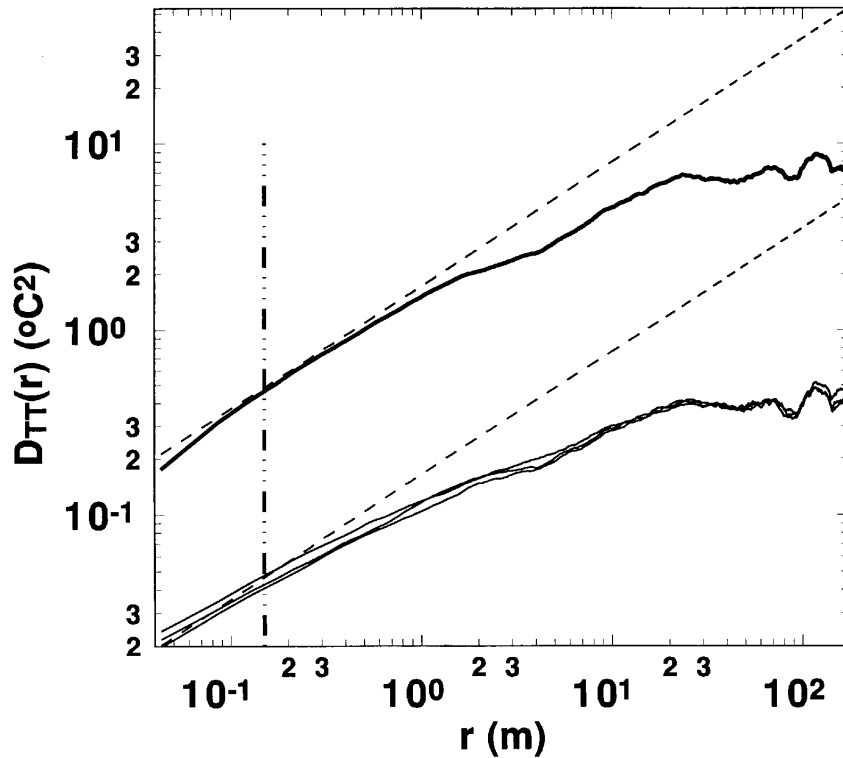


Figure 4b. Same as Figure 4a but for $\langle U \rangle = 1.18 \text{ m s}^{-1}$.

- iv) The interaction in [5] decays very rapidly with decreasing scale suggesting rapid decoupling between the local thermal disturbances and the larger-scale eddy motion. Our analysis does suggest that the local structure of the temperature field is, to a first approximation, uncoupled from the large scale energy containing eddy motion.
- v) While the linear ramp model suggested by Antonia and Van Atta (1978), Antonia *et al.* (1982) and Antonia and Chambers (1978) does address the non-zero values in odd-ordered temperature structure functions, it does not account for any interactions with the local velocity field. Refined ramp models should consider this potential interaction.
- vi) Finally, this study clearly demonstrates that K41 power laws derived from structure function measurements are not very sensitive to the isotropic state of turbulence despite the fact that local isotropy is central to the derivation of these power laws. Our study suggested that local isotropy is not strictly achieved even at scales comparable to $z/2$, but the longitudinal velocity structure function does exhibit a clear $2/3$ power law for scales comparable to $5z$. Also, despite a non-zero structure skewness, the second-order temperature structure

function exhibits a near $2/3$ power law and the normalized velocity-temperature structure function approximately follows Obukhov's (1949) hypothesis.

Acknowledgements

The authors would like to thank Judd Edeburn for his help and support at the Duke Forest and the two reviewers for their helpful comments. Also, the authors greatly appreciate the suggested analysis from one of the anonymous referees for Section 4.3. This project was funded, in part, by the Environmental Protection Agency (EPA) under the co-operative agreement 91-0074-94 (CR817766), and the National Science Foundation (NSF-BIR12333).

Appendix A: Comparison between Triaxial Sonic Anemometer and Thermocouple Temperature Fluctuations

In this appendix, an assessment on how well the Gill triaxial sonic anemometer measures the temperature fluctuations from the fluctuations in the speed of sound is carried out. For that purpose, three Campbell Scientific fine wire thermocouples (diameter = 0.013 mm, expected frequency response 5–10 Hz), situated at $z = 2.6$ m are compared to the triaxial sonic anemometer at $z = 2.75$ m from an experiment carried out in October, 1994 at the same grass clearing. The three thermocouples were situated on a horizontal rod, 1.8 m in length, with two thermocouples on the sides (East–West) of the rod and one thermocouple at the center. The triaxial sonic anemometer was situated 15 cm above the westerly thermocouple.

The data were sampled at 10 Hz for 27.3 minutes ($N = 16,384$ data points) using a 21X Campbell Scientific micrologger and transferred to a 486 Gateway personal computer using an isolated optical interface. The analog output from the Gill sonic anemometer was logged, (which is not of the same quality as the digital data) and the temperature was computed from Equation (4). In Figures 4a and 4b, the temperature structure functions of all four instruments are compared for $\langle U \rangle = 2.16 \text{ m s}^{-1}$, and $\langle U \rangle = 1.18 \text{ m s}^{-1}$, respectively. The Gill temperature structure function measurements are shifted by one decade to permit comparisons for small separation distances. The separation distance was computed from time increments using Taylor's (1938) frozen turbulence hypothesis and the mean horizontal wind speed from the sonic anemometer. These two sample runs were chosen because the wind direction was from the north minimizing mast and other instrument interferences. The $2/3$ power-law is also shown. Notice in Figure 4b that beyond $r = d_{sl}$, the volume averaging by the finite sonic path artificially creates additional dissipation resulting in structure function power-laws much steeper than $2/3$. For $r > d_{sl}$, good agreement between the sonic anemometer temperature measurements

and the fine wire thermocouple is noted, in agreement with an earlier comparison by Katul (1994).

References

- Antonia, R. A. and Van Atta, C. W.: 1975, 'On the Correlation between Temperature and Velocity Dissipation Fields in a Heated Turbulent Jet', *J. Fluid Mech.* **67**, 273–287.
- Antonia, R. A. and Van Atta, C. W.: 1978, 'Structure Functions of Temperature Fluctuations in Turbulent Shear Flows', *J. Fluid Mech.* **84**, 561–580.
- Antonia, R. A. and Chambers, A. J.: 1978, 'Note on the Temperature Ramp Structure in the Marine Surface Layer', *Boundary-Layer Meteorol.* **15**, 347–355.
- Antonia, R. A., Chambers, A. J., Friehe, C. A., and Van Atta, C. W.: 1979, 'Temperature Ramps in the Atmospheric Surface Layer', *J. Atmos. Sci.* **36**, 99–108.
- Antonia, R. A. and Chambers, A. J.: 1980, 'On the Correlation between Turbulent Velocity and Temperature Derivatives in the Atmospheric Surface Layer', *Boundary-Layer Meteorol.* **18**, 399–410.
- Antonia, R. A., Chambers, A. J., and Bradley, E. F.: 1982, 'Relationship Between Structure Functions and Temperature Ramps in the Atmospheric Surface Layer', *Boundary-Layer Meteorol.* **23**, 395–403.
- Antonia, R. A., Anselmet, F., and Chambers, A. J.: 1984, 'Assessment of Local Isotropy Using Measurements in a Turbulent Plane Jet', *J. Fluid Mech.* **163**, 365–390.
- Antonia, R. A., and Kim, J.: 1994, 'A Numerical Study of Local Isotropy of Turbulence', *Phys. Fluids* **6**, 834–841.
- Antonia, R. A., and Zhu, Y.: 1994, 'Inertial Range Behavior of the Longitudinal Heat Flux Cospectrum', *Boundary-Layer Meteorol.* **70**, 429–434.
- Busch, N.: 1973, 'The Surface Boundary Layer, Part I', *Boundary-Layer Meteorol.* **4**, 213–240.
- Bradley, E. F., Antonia, R. A., Chambers, A. J.: 1981, 'Turbulence Reynolds Number and the Turbulent Kinetic Energy Balance in the Atmospheric Surface Layer', *Boundary-Layer Meteorol.* **21**, 183–197.
- Brutsaert, W.: 1982, *Evaporation into the Atmosphere: Theory, History, and Applications*, Kluwer Academic Publishers, 299 pp.
- Fisher, M. J. and Davies, P. O. A.: 1964, 'Correlation Measurements in a Non-Frozen Pattern Turbulence', *J. Fluid Mech.* **18**, 97–116.
- Frisch, U., Sulem, P., and Nelkin, M.: 1978, 'A Simple Dynamical Model of Intermittent Fully Developed Turbulence', *J. Fluid Mech.* **87**, 719–736.
- Gibson, C. H., Friehe, C. A., and McConnell, S. O.: 1977, 'Structure of Sheared Turbulent Fields', *Phys. Fluids* **20**, s156–167.
- Gibson, C. H., Ashurst, W. T., and Kerstein, A. R.: 1988, 'Mixing of Strongly Diffusive Passive Scalars Like Temperature by Turbulence', *J. Fluid Mech.* **194**, 261–293.
- Kader, B. A., Yaglom, A. M., and Zubkovskii, S. L.: 1989, 'Spatial Correlation Functions of Surface-Layer Turbulence in Neutral Stratification', *Boundary-Layer Meteorol.* **47**, 233–249.
- Kaimal, J. C., Wyngaard, J. C., Izumi, Y., and Cote, O. R.: 1972, 'Spectral Characteristics of Surface Layer Turbulence', *Quart. J. Roy. Meteorol. Soc.* **98**, 563–589.
- Kaimal, J. C.: 1986, 'Flux and Profile Measurements from Towers in the Boundary Layer', in D. H. Lenschow (ed.), *Probing the Atmospheric Boundary Layer*, American Meteorological Society, Boston, Massachusetts, pp. 19–28.
- Kaimal, J. C., and Finnigan, J. J.: 1994, *Atmospheric Boundary Layer Flows: Their Structure and Measurements*, Oxford, 289 pp.
- Katul, G. G., Parlange, M. B., and Chu, C. R.: 1994a, 'Intermittency, Local Isotropy, and Non-Gaussian Statistics in Atmospheric Surface Layer Turbulence', *Physics of Fluids* **7**, 2480–2492.
- Katul, G. G.: 1994, 'A Model for Sensible Heat Flux Probability Density Function for Near-Neutral and Slightly-Stable Atmospheric Flows', *Boundary-Layer Meteorol.* **71**, 1–20.

- Katul, G. G., Albertson, J. D., Chu, C. R., and Parlange, M. B.: 1994b, 'Intermittency in Atmospheric Surface Layer Turbulence: The Orthonormal Wavelet Representation', in E. Foufoula-Georgiou and P. Kumar (eds.), in *Wavelets in Geophysics*, Academic Press, 365 pp.
- Katul, G. G., Parlange, M. B., Albertson, J. D., and Chu, C. R.: 1995a, 'Local Isotropy and Anisotropy in the Sheared and Heated Atmospheric Surface Layer', *Boundary-Layer Meteorol.* **72**, 123–148.
- Katul, G. G., Parlange, M. B., Albertson, J. D., and Chu, C. R.: 1995b, 'The Random Sweeping Decorrelation Hypothesis in Stratified Turbulent Flows', *Fluid Dyn. Res.* **16**, 275–295.
- Kerr, R. M.: 1985, 'Higher-Order Derivative Correlations and the Alignment of Small-Scale Structures in Isotropic Numerical Turbulence', *J. Fluid Mech.* **153**, 31–58.
- Kerr, R. M.: 1990, 'Velocity, Scalar, and Transfer Spectra in Numerical Turbulence', *J. Fluid Mech.* **211**, 309–332.
- Kolmogorov, A. N.: 1941, 'The Local Structure of Turbulence in Incompressible Viscous Fluid for Very Large Reynolds Number', *Dokl. Akad. Nauk. SSSR*, **30**, 301–303.
- Kolmogorov, A. N.: 1962, 'A Refinement of Previous Hypotheses Concerning the Local Structure of Turbulence in a Viscous Incompressible Fluid at High Reynolds Number', *J. Fluid Mech.* **13**, 82–85.
- Kuznetsov, V. R., Praskovsky, A. A., and Sabelnikov, V. A.: 1992, 'Fine-Scale Turbulence Structure of Intermittent Shear Flows', *J. Fluid Mech.* **243**, 595–622.
- Landau, L. D., and Lifshitz, E. M.: 1986, *Fluid Mechanics*, Pergamon Press, 539 pp.
- Jayesh, C. Tong, and Warhaft, Z.: 1994, 'On Temperature Spectra in Grid Turbulence', *Phys. Fluids* **6**, 306–312.
- Lin, C. C.: 1953, 'On Taylor's Hypothesis and the Acceleration Terms in the Navier-Stokes Equations', *Q. Appl. Math.* **X**, 154–165.
- Lumley, J. and Panofsky, H.: 1964, *The Structure of Atmospheric Turbulence*, John Wiley and Sons, 229 pp.
- Lumley, J. L.: 1965, 'Interpretation of Time Spectra Measured in High-Intensity Shear Flows', *Phys. Fluids* **8**, 1056–1062.
- Mahrt, L.: 1989, 'Intermittency of Atmospheric Turbulence', *J. Atmos. Sci.* **46**, 79–95.
- Mestayer, P.: 1982, 'Local Isotropy and Anisotropy in a High Reynolds Number Turbulent Boundary Layer', *J. Fluid Mech.* **125**, 475–503.
- Mizuno, T. and Panofsky, H. A.: 1975, 'The Validity of Taylor's Hypothesis in the Atmospheric Surface Layer', *Boundary-Layer Meteorol.* **9**, 375–380.
- Monin, A. S. and Yaglom, A. M.: 1971, *Statistical Fluid Mechanics*, Vol. I, MIT Press, 769 pp.
- Monin, A. S. and Yaglom, A. M.: 1975, *Statistical Fluid Mechanics*, Vol. II, MIT Press, 875 pp.
- Obukhov, A. M.: 1949, 'Local Structure of Atmospheric Turbulence', *Dokl. Akad. Nauk. SSSR* **67**, 643–646.
- Panofsky, H. and Dutton, J.: 1984, *Atmospheric Turbulence: Models and Methods for Engineering Applications*, John Wiley and Sons, 397 pp.
- Pond, S., Stewart, R. W., and Burling, R. W.: 1963, 'Turbulence Spectra in the Wind Over Waves', *J. Atmos. Sci.* **20**, 319–324.
- Powell, D. C. and Elderkin, C. E.: 1974, 'An Investigation of the Application of Taylor's Frozen Hypothesis to Atmospheric Boundary Layer Turbulence', *J. Atmos. Sci.* **31**, 990–1002.
- Praskovsky, A. A., Gledzer, E. B., Karyakin, M. Y., and Zhou, Y.: 1993, 'The Sweeping Decorrelation Hypothesis and Energy-Inertial Scale Interaction in High Reynolds Number Flows', *J. Fluid Mech.* **248**, 493–511.
- Saddoughi, S. G. and Veeravalli, S. V.: 1994, 'Local Isotropy in Turbulent Boundary Layers at High Reynolds Number', *J. Fluid Mech.* **268**, 333–372.
- Sirivat, A. and Warhaft, Z.: 1983, 'The Effect of a Passive Cross-Stream Temperature Gradient on the Evolution of Temperature Variance and Heat Flux in Grid Turbulence', *J. Fluid Mech.* **128**, 323–346.
- Sreenivasan, K. R., Antonia, R. A., and Britz, D.: 1979, 'Local Isotropy and Large Structures in a Heated Turbulent Jet', *J. Fluid Mech.* **94**, 745–775.
- Sreenivasan, K. R.: 1991, 'On Local Isotropy of Passive Scalars in Turbulent Shear Flows', in J. C. R. Hunt, O. M. Phillips and D. Williams (eds.), *Turbulence and Stochastic Processes: Kolmogorov's Ideas 50 Years On*, Roy. Soc. 240 pp.

- Stull, R.: 1988, *An Introduction to Boundary Layer Meteorology*, Kluwer Academic Publishers, 666 pp.
- Taylor, G. I.: 1938, 'The Spectrum of Turbulence', *Proc. Roy. Soc. A* **1164**, 476–490.
- Tennekes, H. and Lumley, J. L.: 1972, *A First Course in Turbulence*, MIT Press, 300 pp.
- Townsend, A. A.: 1976, *The Structure of Turbulent Shear Flow*, Cambridge University Press, 429 pp.
- Van Atta, C. W.: 1977, 'Effect of Coherent Structures on the Structure Functions of Temperature in the Atmospheric Boundary Layer', *Arch. Mech.* **29**, 161–171.
- Wyngaard, J. C. and Clifford, S. F.: 1977, 'Taylor's Hypothesis and High Frequency Turbulence Spectra', *J. Atmos. Sci.* **34**, 922–929.
- Wyngaard, J. C.: 1981, 'Cup, Propeller, Vane, and Sonic Anemometer in Turbulence Research', *Ann. Rev. Fluid Mech.* **13**, 922–929.